February 2001

A Microcantilever Device to Assess the Effect of Force on the Lifetime of Selectin-Carbohydrate Bonds

Davis F. J. Tees
University of Pennsylvania

Richard E. Waugh
University of Rochester

Daniel A. Hammer
University of Pennsylvania, hammer@seas.upenn.edu

Reprinted from *Biophysical Journal*, Volume 80, Issue 2, February 2001, pages 668-682.
Publisher URL: http://www.biophysj.org/cgi/reprint/80/2/668

A Microcantilever Device to Assess the Effect of Force on the Lifetime of Selectin-Carbohydrate Bonds

Abstract

A microcantilever technique was used to apply force to receptor-ligand molecules involved in leukocyte rolling on blood vessel walls. E-selectin was adsorbed onto 3-μm-diameter, 4-mm-long glass fibers, and the selectin ligand, sialyl Lewis^x, was coupled to latex microspheres. After binding, the microsphere and bound fiber were retracted using a computerized loading protocol that combines hydrodynamic and Hookean forces on the fiber to produce a range of force loading rates (force/time), r_f. From the distribution of forces at failure, the average force was determined and plotted as a function of ln r_f. The slope and intercept of the plot yield the unstressed reverse reaction rate, k_r^o , and a parameter that describes the force dependence of reverse reaction rates, r_o. The ligand was titrated so adhesion occurred in ~30% of tests, implying that >80% of adhesive events involve single bonds. Monte Carlo simulations show that this level of multiple bonding has little effect on parameter estimation. The estimates are r_o = 0.048 and 0.016 nm and k_r^o = 0.72 and 2.2 s^{-1} for loading rates in the ranges 200–1000 and 1000–5000 pN s^{-1}, respectively. Levenberg-Marquardt fitting across all values of r_f gives r_o = 0.034 nm and k_r^o = 0.82 s^{-1}. The values of these parameters are in the range required for rolling, as suggested by adhesive dynamics simulations.

Comments

Reprinted from *Biophysical Journal*, Volume 80, Issue 2, February 2001, pages 668-682.
Publisher URL: http://www.biophysj.org/cgi/reprint/80/2/668

A Microcantilever Device to Assess the Effect of Force on the Lifetime of Selectin-Carbohydrate Bonds

David F. J. Tees,* Richard E. Waugh,† and Daniel A. Hammer*

*Department of Chemical Engineering and Institute of Medicine and Engineering, University of Pennsylvania, Philadelphia, Pennsylvania 19104; and †Department of Pharmacology and Physiology, University of Rochester, Rochester, New York 14642 USA

ABSTRACT A microcantilever technique was used to apply force to receptor-ligand molecules involved in leukocyte rolling on blood vessel walls. E-selectin was adsorbed onto 3-μm-diameter, 4-mm-long glass fibers, and the selectin ligand, sialyl Lewis^x, was coupled to latex microspheres. After binding, the microsphere and bound fiber were retracted using a computerized loading protocol that combines hydrodynamic and Hookean forces on the fiber to produce a range of force loading rates (force/time), r_f. From the distribution of forces at failure, the average force was determined and plotted as a function of ln r_f. The slope and intercept of the plot yield the unstressed reverse reaction rate, k_r^o, and a parameter that describes the force dependence of reverse reaction rates, r_o. The ligand was titrated so adhesion occurred in ~30% of tests, implying that >80% of adhesive events involve single bonds. Monte Carlo simulations show that this level of multiple bonding has little effect on parameter estimation. The estimates are r_o = 0.048 and 0.016 nm and k_r^o = 0.72 and 2.2 s^{-1} for loading rates in the ranges 200–1000 and 1000–5000 pN s^{-1}, respectively. Levenberg-Marquardt fitting across all values of r_f gives r_o = 0.034 nm and k_r^o = 0.82 s^{-1}. The values of these parameters are in the range required for rolling, as suggested by adhesive dynamics simulations.

INTRODUCTION

Adhesion between biological macromolecules is important in many biological phenomena, including angiogenesis (Bischoff, 1997), blood clotting (Colman et al., 1994), cancer metastasis (Lafrenie et al., 1993), and inflammation (Springer, 1994). The receptor-ligand bonds form between proteins and carbohydrates that interact at binding sites determined by the three-dimensional structure of the molecules. Thermal energy from the aqueous medium can overcome the bonding potential that is the sum of hydrophobic interactions, hydrogen bonds, and electrostatic interactions between charged, polar, or hydrophobic amino acid side chains in the binding interface. Bond dissociation occurs stochastically with a characteristic bond lifetime, t_o, that is the reciprocal of the reaction limited reverse reaction rate, k_r^o (Bell, 1978).

A major area of interest for bioadhesion research is the attachment and arrest of cells on blood vessel walls in circulation (Springer, 1994). This process occurs in the dynamic environment of flowing blood, and so the effect of hydrodynamic forces on rate constants for cell attachment and dissociation has become the subject of recent investigation (Bruinsma, 1997). The selectin family of adhesion molecules mediates the rolling adhesion of white blood cells to endothelial cells lining blood vessel walls (Kansas, 1996). Selectin-mediated adhesion is essential for facilitating white blood cell attachment to the vessel wall at physiological shear rates even though these molecules are less efficacious than integrins, which are required for firm adhesion, in static assays of binding (Lawrence and Springer, 1991; von Andrian et al., 1991). It is known that the bonding interaction between the molecules themselves is a sufficient condition for rolling, since rolling can occur in a completely reconstituted system consisting of selectins bound to glass surfaces and carbohydrates coated on latex beads (Brunk et al., 1996; Brunk and Hammer, 1997). Other cell-related phenomena, such as signaling or cell deformability, may serve a regulatory role, but are not required for the rolling phenotype to be observed. It has also been suggested that differences in the force dependence of reverse reaction rates of the bonding molecules can account for the rolling versus firm adhesion phenotypes (Dembo et al., 1988; Hammer and Apte, 1992).

The first expression for the force dependence of bond lifetime to gain wide currency was proposed in a seminal paper by Bell (1978):

$$k_r(f) = k_r^o \exp[r_o f/k_B T]. \quad (1)$$

Here, $k_r(f)$ is the bond reverse reaction rate as a function of force, k_r^o is the reverse reaction rate in the absence of applied force, f is the applied force per bond, k_B is the Boltzmann constant, T is absolute temperature, and r_o is a parameter with units of length that describes how strongly the reaction rate changes with force. Other models have since been proposed (Dembo et al., 1988; Evans et al., 1991). A recent paper from the Evans group (Evans and Ritchie, 1997) used transition state theory (Kramers, 1940; Hänggi et al., 1990) in the presence of applied forces to show that the effect of applied force on the energy barrier height can be calculated from a given potential of mean force. None of these models,

Received for publication 15 July 1999 and in final form 15 November 2000.

Address reprint requests to Daniel A. Hammer, Department of Chemical Engineering, 311A Towne Bldg., University of Pennsylvania, 220 S. 33rd St., Philadelphia, PA 19104. Tel.: 215-573-6761; Fax: 215-573-2903; E-mail: hammer@seas.upenn.edu.

0006-3495/01/02/668/15 $2.00

however, has yet been thoroughly validated for cell adhesion molecules.

A number of methods have been used to apply forces to small numbers of receptor-ligand bonds. Hydrodynamic forces can be used to apply force to doublets of adherent cells in suspension (Tha et al., 1986; Tees et al., 1993) or to cells adhering to the surface of a flow chamber (Alon et al., 1995; Pierres et al., 1995; García et al., 1998; Brunk and Hammer, 1997). In each of these cases the applied force can be calculated after some plausible assumptions about the location of bonds in the contact area are made. Alon et al. (1995) used the tether duration distribution of white blood cells interacting with ligand-coated surfaces at different shear stresses to measure the k_r^o and r_o Bell model parameters for P-selectin/PSGL-1 binding (and later for the other selectins (Alon et al., 1997)). The assumptions made in these methods, however, reduce the accuracy with which molecular parameters can be determined, thus requiring independent methods of measurement.

Atomic force microscopy (AFM), which uses a calibrated, oscillating, needle-tipped cantilever to form and apply force to receptor-ligand bonds, is a potentially powerful tool for applying forces to small numbers of bonds (Radmacher et al., 1994; Florin et al., 1994). A number of groups have found protocols that allow AFM to be applied in ways that allow the force dependence of dissociation to be determined (Hinterdorfer et al., 1996; Fritz et al., 1998). An alternative device for measuring picoNewton forces is the biomembrane force probe (Evans et al., 1991; Merkel et al., 1999). This device consists of a calibrated biomembrane (usually a red blood cell), coated with receptor, held in a micropipette, and apposed to a ligand-covered surface. Several groups have used this technique successfully to apply forces to avidin-biotin bonds (Merkel et al., 1999) as well as Fcγ receptor IIIA-IgG bonds (Chesla et al., 1998). Other useful picoNewton-force application work has been performed by repeatedly forcing cells into contact with antibody-coated beads using micropipette suction (Shao et al., 1998).

Another important factor in attempts to measure the force dependence of reaction rates is the inevitability of force loading profiles in any experiment (Evans and Ritchie, 1997). In the simplest experiment, the lifetime of bonds instantly exposed to a constant force would be measured. In reality, however, it is never possible to apply a force instantaneously; there is always a finite loading rate, r_f. In AFM, bonds are exposed to a constant linear ramp of force as the cantilever is retracted over a millisecond time scale. In the neutrophil tethering experiment (Alon et al., 1997), the loading rate is reflected in the time for bonds to move to the back of the contact area and experience loading as microvilli and molecules are stretched by shear stress. The typical scale of these loading rates is ~100 pN applied on a time scale of 10–1000 ms. Thus, to cover the range of force loading rates important for circulation, loading rates from 10^2 to 10^4 pN s^{-1} must be examined.

Evans and Ritchie (1997) describe a method for calculating parameters in the Bell model that takes advantage of finite loading rates. From reliability theory (Beckmann, 1967), the probability, $p(t, f)$, of a single bond dissociating in the interval $(t, t + dt)$ as a function of force is:

$$p(t, f) = k_r(f) \exp\left\{-\int_o^t k_r(f(t'))dt'\right\}. \quad (2)$$

The first term represents the probability of dissociation in the next short interval of time, dt, whereas the exponential term represents the probability of the bond having survived up to time, t. The time (and hence the force, f_{crit}) corresponding to the mode, or peak value in this probability distribution can be found by setting $\partial p/\partial f = 0$ and using the linear ramp of force, $f(t) = r_f t$, (where r_f is the force loading rate) to express the integral in terms of f and df. One then obtains:

$$k_r(f_{crit}) = r_f \frac{\partial}{\partial f} \ln k_r(f)|_{f=f_{crit}}. \quad (3)$$

If the Bell model (Eq. 1) is substituted into Eq. 3, then after some rearrangement:

$$f_{crit} = \frac{kT}{r_o} \ln\left(\frac{r_o}{k_r^o kT}\right) + \frac{kT}{r_o} \ln r_f. \quad (4)$$

Thus, the relationship between f_{crit} and $\ln r_f$ is linear with slope and intercept given by:

$$\text{slope} = \frac{kT}{r_o}; \quad \text{intercept} = \frac{kT}{r_o} \ln\left[\frac{r_o}{k_r^o kT}\right]. \quad (5)$$

The Bell model parameters r_o and k_r^o can, thus, be calculated from the slope and intercept of f_{crit} versus $\ln r_f$ (Merkel et al., 1999).

In the present paper, the above analysis is used to derive the parameters for the Bell model using a technique that employs a long, thin glass fiber as an elastic force transducer. This technique has been used previously to pull membrane tethers from red blood cells (Hwang and Waugh, 1997). The force loading can be easily controlled and the force transducing system produces fiber deflections that are large enough to be visible under the microscope while still producing picoNewton scale forces.

The device is used to apply forces to E-selectin/carbohydrate bonds. To elucidate the bonding interactions in the cell-free rolling experiments described above, the same system of E-selectin adsorbed to glass fibers and carbohydrate coupled to latex beads was employed.

MATERIALS AND METHODS

Adhesion molecules

A chimeric form of human E-selectin (comprising two amino terminal consensus repeat domains, the epidermal growth factor domain and the lectin domain of E-selectin, attached to each arm of a mouse IgG_1 antibody) was the generous gift of Dr. Ray Camphausen of the Genetics Institute (Cambridge, MA). Sialyl Lewis^x (sLe^x), the low-affinity tetrasaccharide ligand for E-selectin (Varki, 1994) was purchased in multivalent form (Glycotech, Rockville, MD). SLe^x groups are attached to a polyacrylamide (PAA) backbone by substitution of a fraction of the polymer side chain. An additional fraction of the side chains are replaced with biotin for binding of the polymer to streptavidin-coated surfaces. The polymer molecular weight is ~30 kd. There are ~20 sugar groups and ~4 biotin groups/polymer. A similar multivalent form of the trisaccharide Lewis^x (Le^x), which does not mediate adhesion to E-selectin in flow (Brunk and Hammer, 1997), was also purchased (Glycotech). For adhesion blocking experiments, the anti-E-selectin blocking antibody (BBA2, mouse IgG_1, R&D Systems, Minneapolis, MN) was used.

Construction and processing of microcantilevers

Three-μm-diameter uniform E-glass fibers (MO-SCI Corp., Rolla, MO) were trimmed to lengths of 2 to 5 mm, inserted into the tips of micropipettes (~7 μm diameter), and secured with UV curing adhesive (NOA 71; Norland Inc., New Brunswick, NJ) under a low power dissecting microscope. The adhesive was cured overnight under 365 nm UV illumination (Spectroline E-series; Spectronics Corp., Westbury, NY).

For incubation with E-selectin, the pipettes that hold the fibers were inserted through specially modified pipette holders (MPH-1; E. W. Wright, Guilford, CT) with a protective 2-mm outside diameter glass sleeve inserted into one end. The glass sleeves were inserted into the drilled-out tops of 1.5 ml siliconized polypropylene tubes (Marsh Biomedical Products, Inc., Rochester, NY), and the holder was cemented to the tube top with silicone sealant. By retracting the fiber into the protective sleeve, the fiber was protected from damage during washing steps. For incubation, the fiber was pushed out into the solution in the tube. After adsorption with selectin, the fiber was retracted into the protective sleeve, the tube cap was cut from the tube, and the holder was placed into a clip atop a manipulator assembly that allowed 5 degrees of freedom for positioning the fiber tip in the microscope field of view. The fiber tip was then pushed out of its protective sleeve into the viewing chamber.

E-selectin adsorption to glass fibers

Fibers were washed overnight in sterile filtered 0.1 M phosphate buffered saline (PBS; pH 6.6) at 4°C. The next day, the buffer was discarded and the holder tubes were washed twice with fresh PBS buffer. Each tube was filled with 750 μl of 0.1–10.0 μg ml^{-1} E-selectin chimera in PBS+ (PBS with 0.9 mM $CaCl_2$ and 0.5 mM $MgCl_2$, pH 6.6). The concentration of E-selectin was varied to find the amount that led to significant numbers of adhesive events during the apposition experiments described below. The concentration of E-selectin was 2 μg ml^{-1} in all of the experiments used to produce Figs. 8 and 9. The fibers were incubated for 2 h at room temperature on an orbitron rotator (Boekel Instruments, Feasterville, PA). The fibers were washed twice with PBS+ (pH 7.4) then incubated in 1 ml of 1.0% (wt/wt) bovine serum albumin (BSA) in PBS+ (pH 7.4; denatured for 30 min at 57°C) on the orbitron rotator for 30 min at room temperature. Finally, the holder tubes and fibers were washed twice with sterile filtered PBS+ containing 1% denatured BSA. The fibers were stored in this medium until use.

The spring constant for the fiber was calculated from the fiber dimensions. The Hookean spring constant, k_{fiber}, for deflection of a thin beam is given by Moore et al. (1989):

$$k_{\text{fiber}} = \frac{3\pi}{64}\frac{ED^4}{L^3}, \tag{6}$$

where D is the fiber diameter, L is the fiber length, and E is the modulus of elasticity for E-glass (= 74 ± 2 × 10^{10} N · m^{-2}; average from the literature: Jones, 1994; Gibson, 1994; Hyer, 1998).

Preparation of sLe^x coated microspheres

Streptavidin-coated polystyrene latex microspheres 10.4 μm in diameter were purchased from Bangs Labs (cat. no. C0104000RN; Fishers, IN). Ten microliters of these beads were washed three times with 1 ml PBS+/1% BSA/0.01% NaN_3 for a final concentration of 2.0 × 10^4 sphere ml^{-1}. Multivalent sLe^x was added at a final concentration of 0.5 μg ml^{-1} and incubated with the microspheres at room temperature for 45 min, with periodic vortexing. The concentration of sLe^x on the microsphere was titrated by diluting the sLe^x-PAA-biotin with Le^x-PAA-biotin, which does not bind to E-selectin in flow. The optimum titration for apposition experiments was found to be 20% sLe^x and 80% Le^x by volume in the incubation solution. The spheres were washed three times and finally resuspended in 1 ml PBS+/1% BSA/0.01% NaN_3 before use. Spheres and fibers were always used the day they were made, and media were prepared freshly for each experiment.

Tests for adsorption of E-selectin

To test for the presence of E-selectin, enzyme-linked immunosorbent assay (ELISA) was performed on the fibers by incubating them first with an anti-E-selectin monoclonal antibody (BBA2, mouse IgG_1, R&D Systems) and then, after extensive washing, with an alkaline phosphatase-conjugated sheep anti-mouse IgG_1 antibody (AACO2A Harlan Serotec, Indianapolis, IN). The fibers were moved to fresh holder tubes and immersed in the substrate for alkaline phosphatase (Sigma 104, Sigma, St. Louis, MO) in pH 9.8 diethanolamine buffer overnight at 4°C. This step was made necessary by the discovery that E-selectin adsorbed strongly to the walls of the tubes, producing a large background color within seconds of addition of substrate. Blocking the tubes with BSA prior to the assay had no effect on this adsorption. Immersing the fibers in fresh tubes allowed the effect of the fiber alone to be seen, but a 14-h incubation at 4°C was required to produce enough color for detection. The optical density at 405 nm (OD_{405}) was measured in a spectrophotometer (Spectronic 1001 plus, Milton Roy, Rochester, NY) and used as a relative measure of the amount of selectin bound to the fiber. The signal was found to be repeatable with a small dependence on pH. The optimal pH for attachment was found to be 6.6. When incubation with either the first (anti-E-selectin) or second (alkaline phosphatase-conjugated anti IgG_1) antibody was omitted, the OD_{405} was the same as the OD_{405} for Sigma 104 in diethanolamine buffer (the reference used to set zero on the spectrophotometer).

Apposition Experiments

All experiments were conducted at room temperature. Microspheres suspended in PBS+/1% BSA/0.01% NaN_3 were introduced into a viewing chamber on a custom built stage attached to an inverted microscope (Nikon Diaphot 300; Optical Apparatus Co., Ardmore, PA). The microspheres were aspirated onto the tips of 4- to 7-μm-inner diameter micropipettes using an aspiration pressure of 1.0 cm of H_2O produced with a custom-built manometer. Pressure was transduced by coarse (DP15; 0–100 cm of H_2O) and fine (DP103; 0–2 cm of H_2O) pressure transducers (Validyne Corp., Northridge, CA). The micropipette was mounted in series with a piezoelectric actuator equipped with position feedback to eliminate hysteresis

(17PAZ007; Melles Griot, Boulder, CO). The actuator was controlled using a GP-IB interface driven with Labview 4.0 on a 200 MHz Pentium Pro computer (Gateway 2000, N. Sioux City, SD) and could be retracted its full 30-μm travel in less time than is recorded by a single video frame (33 ms).

For initial positioning and the manipulation of the microsphere, the actuator and pipette were mounted on a 5:1 water-driven micromanipulator (Narishige MMW22; Optical Apparatus Co.). This was mounted, in turn, on a coarse manipulation system (Newport Corp., Irvine, CA), allowing control over all translational and rotational degrees of freedom. The entire assembly was mounted on a vibration isolation table (TMC, Peabody, MA).

The bead and fiber were viewed through the microscope with a 40× 0.55 NA objective and sufficient empty magnification to ensure that the 30-μm actuator deflection covered the entire imaging surface of a CCD video camera (CCU-84; Pulnix, Sunnyvale, CA). The video signal from the camera was merged with time, date, and aspiration pressure data using a video encoder (Department of Biophysics, University of Rochester, Rochester, NY). The resulting signal was displayed on a video monitor (Panasonic TR930B, Matsushita Electric Corp., Osaka, Japan), and recorded on S-VHS videocassette (Sony SVO-9500; Optical Apparatus Co.).

In a typical experiment, a bead was aspirated and manipulated into contact with the fiber using the Narishige micromanipulator. The fiber was given a small initial negative deflection (<1 μm) to ensure that bead and fiber were in contact. The computer was set to produce a known deflection (typically 20 μm) in a set time (0.01–10 s). This allowed a range of force-loading rates to be produced. An apposition protocol consisted of the following stages: 1) apposition—the bead was held in contact with the fiber for a set period of time; 2) retraction—the bead was retracted at a set loading rate for a certain distance; 3) hold—the retracted position was held for a set period of time to allow the fiber to relax back to its rest position; and 4) return—the bead was returned to its initial position in contact with the fiber. The retraction phase was generally 1.0 s long, although retraction times of 2.0 or 5.0 s were used for some slow loading rate experiments. This almost always allowed sufficient time for the bonds to break. The 4% of events that survived to the hold phase were excluded from the computation of the average force at break-up, since they did not dissociate during exposure to the linear force loading. The hold phase was 2 to 5 s in duration, depending on the time required for the fibers to relax to their rest position.

A sequence of video frames taken during an adhesive event is shown in Fig. 1. The fiber appears to hang down vertically from the top of the frame, and the fiber tip is visible at the bottom. The 10-μm-diameter bead can be seen held by the micropipette using a small suction pressure (1.0 cm of H_2O) which was kept constant throughout the experiment. This pressure was always enough to hold the bead firmly on the pipette during adhesive events. Using the micromanipulator, the bead was positioned 10 to 40 μm from the fiber tip. The fiber was brought into focus, and the bead was manipulated into the same focal plane. To further ensure the exact alignment of the bead and fiber, the bead was used to push the fiber gently past its rest position. As the bead was moved into and out of the plane of focus, the fiber deflected along the bead's curved surface. When the bead and fiber were exactly aligned, the maximum fiber deflection occurred.

In each experiment, hundreds of apposition cycles were performed and recorded on videotape for analysis. The events were analyzed frame by frame by capturing images with a frame grabber board (PCI 1408; National Instruments, Austin, TX) and analyzing them with Labview and IMAQ Vision (National Instruments). The videotape was advanced frame by frame and paused during capture using a serial interface under computer control from the analysis program. The image was thresholded and filtered to remove noise using image analysis tools (IMAQ Vision; National Instruments). The instantaneous fiber position was found by taking the average horizontal position of non-zero pixels in a thresholded image along three horizontal TV lines at the top and bottom of the image. The fiber position was determined to within 1 to 2 pixels by finding the average position of pixels above threshold along the selected image lines. The

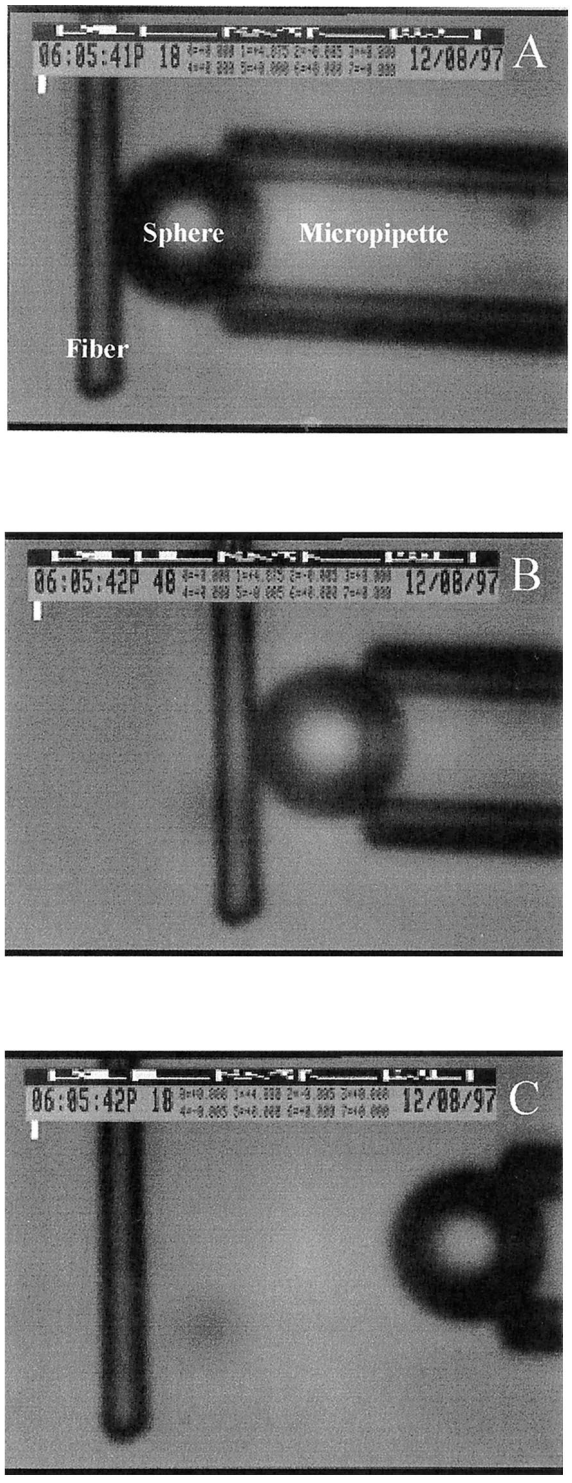

FIGURE 1 A sequence of video frames from an adhesive event. In frame *A*, the bead and fiber are apposed, with the fiber given a small negative displacement with respect to its rest position (frame *C*). In frame *B*, the micropipette is retracted and a bond between bead and fiber leads to positive deflection of the fiber. Immediately after this frame, the bond dissociated. Frame *C* shows the bead and fiber in their final rest positions.

centroid of the microsphere was determined using an analysis routine that finds circles of a given size. Length calibration was accomplished by capturing and measuring the image of a stage micrometer. For the magnification used, one pixel corresponded to 59 nm, and thus the centroid of the fiber could be determined to within ~100 nm, much better than optical resolution.

Fig. 2 shows a trace of the sphere and fiber positions as a function of time from frame by frame image analysis using a high density of E-selectin to obtain a high percentage of adhesive events (% adhesion). The first seven bead appositions led to spikes in the fiber position that represent adhesive events of varying duration. The final apposition test did not result in a bond. The fraction of tests leading to adhesive events in this example was, thus, 7/8 (87.5%) adhesion. (In experiments to determine the average force at breakup, $\langle F_{break} \rangle$, lower selectin densities were used to obtain lower % adhesion). It is important to note that the spikes were not all the same height. Given that the fiber deflection was related to the applied force on the bonds at the moment of breakup, this demonstrates that the bonds do not break the instant a well-defined failure force is exceeded.

In the experiments for which data are reported, the concentration of biotinylated sLe^x on the beads was reduced (by titration with biotinylated Le^x) so that the rate of bond formation was only 25–30%. In all our experiments, the background of nonspecific events was 4–9% of all tests. To ensure that most events were mediated by E-selectin and sLe^x binding, a rate of ~30% adhesion was sought. This rate implies that 70% of tests ended with no bond formation (i.e. the number of bonds, $N_b = 0$). Poisson distribution statistics (Merkel et al., 1999; Chesla et al., 1998) then imply that when 30% of tests have $N_b > 0$, there will be 83% single bonds ($N_b = 1$), 15% will be double bonds ($N_b = 2$), and <3% will have $N_b > 2$. For more explanation of this very important point, see Appendix A.

Tests for specificity

Three sets of experiments were performed to test for the prevalence of nonspecific interactions between polystyrene beads and glass surfaces. In the first set, the beads were coated with sLe^x or Le^x, but the fibers were coated with only albumin without previous selectin incubation (sLe^x-BSA and Le^x-BSA). In the second set of experiments, the fibers were coated with E-selectin but the beads were conjugated with Le^x, a trisaccharide similar to sLe^x but lacking the sialic acid residue and not a ligand for E-selectin. In the third set, both bead and fiber were conjugated with sLe^x and E-selectin as usual, but the interaction was blocked with a monoclonal anti-E-selectin adhesion blocking antibody. The result of running many test appositions (the number in parentheses above each column) with these different blocking protocols is shown in Fig. 3. The first column shows the positive result using the E-selectin chimera-coated fibers and sLe^x-coated beads. For the high concentrations of sLe^x and E-selectin used for these demonstration experiments, 55% of apposition tests led to adhesive events. When blocking antibody was added, the percentage fell to 23%, a decrease that was statistically significant ($P < 0.001$). The background levels of nonspecific binding using Le^x-E-selectin, sLe^x-BSA, and Le^x-BSA were 3.0, 8.8, and 4.8%, respectively, significantly below what is seen with sLe^x-E-selectin interactions.

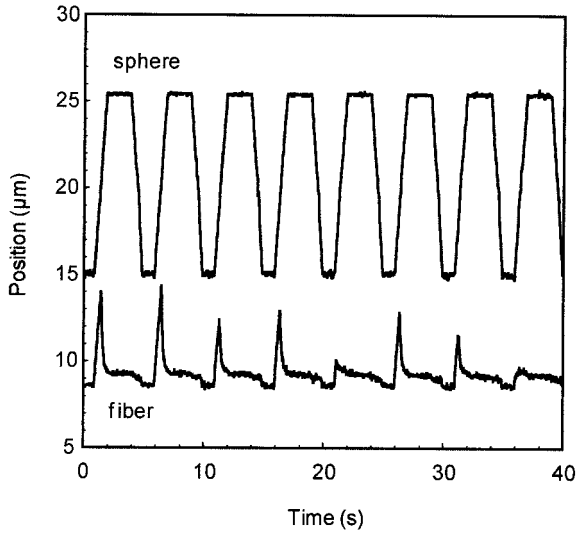

FIGURE 2 Trace of sphere and fiber position versus time from frame-by-frame image analysis. The upper trace shows the position of the sphere center. The bottom trace shows the position of the fiber. Initially, in each cycle, the two are in contact. The sphere and fiber retract together until the moment of bond dissociation when the fiber returns to its rest position and the sphere continues retracting until it comes to rest (10 μm from its starting point). Tests 1–7 resulted in adhesive events of varying maximum deflection. The final test was a non-event and shows only hydrodynamic deflection.

Determination of fiber spring constants

A calibration of the fiber spring constant was performed to test the validity of Eq. 6 and determine an experimental value for the Young's modulus of the E-glass cantilevers used in the experiments. A biotinylated gelatin emulsion was formed by mixing and repeatedly aspirating through a double-ended 22-gauge luer-lock needle a solution containing 40 mg ml^{-1}

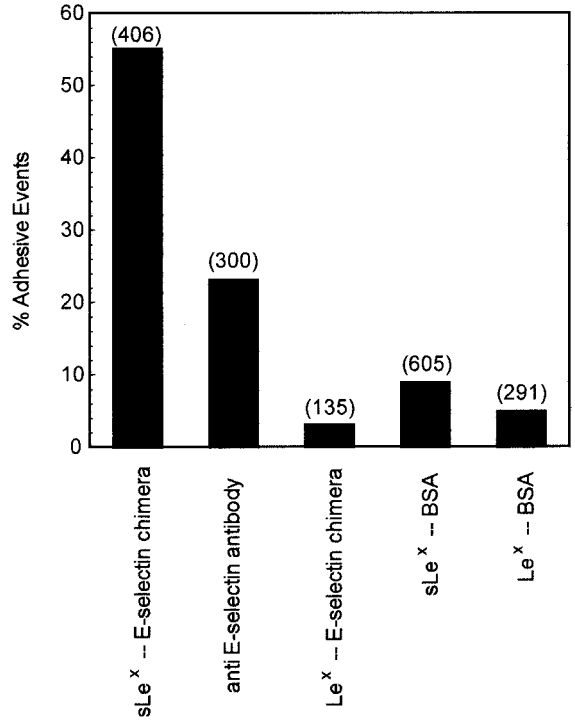

FIGURE 3 Chart of E-selectin-sLe^x bonding specificity tests. The first column shows the percentage of apposition tests that led to adhesive events for sLe^x-E-selectin chimera binding. Use of E-selectin blocking antibody (*column 2*), Le^x instead of sLe^x (*column 3*) or BSA in place of E-selectin (*columns 4 and 5*) all reduce the frequency of adhesive events significantly ($p < 0.001$). The number in parentheses above each column is the number of apposition tests used for the computation of percentage of adhesive events.

gelatin (G9391; Sigma Chemical Co.) and 20 mg ml^{-1} of water soluble sulfo-NHS-LC-biotin (Pierce, Rockford, IL) in PBS+. The tips of 15 fibers were coated by repeated immersion in emulsion followed by fixation with formalin vapor for 45 min. The gelatin coating is smooth and invisibly thin under light microscopy. Approximately 10 μl of red blood cells (RBC) were collected by fingerprick into a heparinized capillary tube. The RBC were washed three times with PBS+ (no BSA; pH 7.4), then biotinylated with sulfo-NHS-LC-biotin at a final concentration of 1.5 mg/ml for 1 h. The RBC were washed twice with PBS+ (no BSA), then twice more with PBS+/1% BSA/0.1% NaN_3 (pH 7.4). Ten μl of 2 μm-diameter streptavidin-coated latex beads (Interfacial Dynamics Corporation, Portland, OR) were washed three times with PBS+/1% BSA/0.1% NaN_3 (pH 7.4). A mixture was prepared containing 6400 latex beads/μl and 5200 RBC/μl in 1 ml PBS+/1% BSA/0.1% NaN_3 (pH 7.4) and mixed for 1 h on a rotary mixer to form RBC/bead pairs.

RBC/bead pairs were bound to the cantilever, and the RBC was completely aspirated into pipettes of radius R_p = 2.7–3.0 μm to form a piston in the pipette. A fixed aspiration pressure, ΔP, was set using a manometer and the equilibrium fiber deflection, x, required to balance the aspiration pressure and prevent the red cell from being sucked in or pulled out of the pipette was recorded. The suction force, $F_{suction}$, acting on the red cell piston, and hence on the fiber, is given by: $F_{suction} = \pi R_p^2 \Delta P = k_{spring} x$. Sample fiber deflection versus $F_{suction}$ curves are shown in Fig. 4 *a* for three different fibers. The slope of each curve gives the respective fiber spring constant. Experimental spring constants were obtained for 15 fibers. The spring constant of each fiber was determined using two or more red cell pistons to ensure consistency. The average ratio of experimental to calculated fiber spring constant from 37 test data sets was 0.97 ± 0.25. The error in this correction factor is consistent with the random error expected from propagation of the 3–4% errors in L and D through Eq. 6. The experimental Young's modulus was corrected using this factor to 72×10^{10} N · m^{-2}. Using this value, Eq. 6 was used to determine the spring constants of fibers used in the apposition experiments.

Correction of the fiber force for hydrodynamic drag

Fibers pulled through a viscous medium experience hydrodynamic forces. The force on a fiber in a uniform flow field, U, has been derived (Cox, 1970; Batchelor, 1970). For a freely suspended, finite-length high-aspect-ratio fiber of circular cross-section exposed to a flow perpendicular to its long axis, the force perpendicular to the fiber axis is given by Cox (1970; Eqs. 8.1 and 8.2):

$$F_{hydro} = \frac{4\pi\mu UL}{\ln(2L/D) - 0.5 + \ln 2}, \tag{7}$$

where μ is the fluid viscosity, U is the flow velocity, L is the fiber length, and D is the fiber diameter. The fibers used in our experiments are not freely suspended: the tip of the micropipette into which the fibers are glued does not move when the fiber is deflected, and thus one fiber end is effectively clamped. The free end, however, experiences only very small angular deflections (<0.6°), and thus the Cox expression should provide a reasonable estimate for the hydrodynamic drag on a fiber when the tip is deflected at speed U (to within some correction factor g to account for the clamped end and the presence of boundaries).

One can estimate the parameter g from observation of the decay of fiber position to the undeflected position after a large adhesive event. In the fiber deflection curves (Fig. 2) the fiber clearly does not snap back instantaneously, but instead returns to its rest position slowly. During the return there is a balance between the elastic restoring force of the fiber, F_{Hooke}, = $k_{fiber}x$, (where k_{fiber} is defined in Eq. 6 and x is the fiber deflection from rest) and the effective hydrodynamic drag, $F_{hydro} = aU$ (where the parameter a includes the correction factor g and all the factors on the right-hand side of Eq. 7 except the velocity):

$$F_{applied} = k_{fiber}x + aU = 0. \tag{8}$$

After release, the applied force is zero. Also note that the velocity U is dx/dt, so the time course for the return of the fiber to its rest position is the solution to a first order differential equation:

$$x = x_{max} \exp[-(k_{fiber}/a)t], \tag{8a}$$

where x_{max} is the maximum fiber deflection at the point of bond dissociation and t is time after the bond dissociates. Thus if ln x is plotted versus t, the negative of the slope of the resulting line will give k_{fiber}/a. If k_{fiber} is known, then a can be calculated and compared to the theoretical value predicted by Cox (1970).

Constant-force loading rate protocol

Measurement of the effective hydrodynamic drag on the fiber made it possible to include this effect in the force balance during retraction so that a constant ramp of force with any value could be produced. For a constant force loading rate in the presence of hydrodynamic and Hookean forces, the desired force balance is given by:

$$k_{fiber}x + a\frac{dx}{dt} = r_f t + f_o \tag{9}$$

Here, f_o is the applied force on the fiber at $t = 0$. The fiber is given a small negative deflection initially, $-x_o$, and this initial negative force can be introduced into the loading protocol using $f_o = -k_{fiber}x_o$. This equation is easily solved using the multiplying factor $\exp[(k_{fiber}/a)t]$. For the required initial condition $x = -x_o$ at $t = 0$, the fiber position, $x(t)$ follows the equation:

$$x = \frac{r_f}{k_{fiber}}t - x_o - \left(\frac{r_f}{k_{fiber}}\right)\left(\frac{a}{k_{fiber}}\right)\left[1 - \exp\left\{-\frac{k_{fiber}}{a}t\right\}\right]. \tag{10}$$

It may be verified that the required velocity is zero at $t = 0$, and goes to r_f/k_{fiber} as $t \to \infty$. This expression was programmed into the piezo retraction protocol using Labview.

RESULTS

Hydrodynamic forces on fibers

Observation of the time course of the fiber returning to its resting state after release enabled calculation of the effective hydrodynamic drag force on the fiber. Fig. 4 *b* shows the results of such an analysis for three events obtained using the same fiber. After an initial period ($t < 0.2$ *s*) when some of the slopes are shallower, the values become very consistent, leading to $k_{fiber}/a = 3.00 \pm 0.11$ s^{-1}. For this fiber, L = 4.1 mm and D = 3.2 μm, so k_{fiber} = 16.6 pN μm^{-1}, and hence a = 5.52 pN s μm^{-1}. For this aspect ratio, a_{Cox} = 6.4 pN s μm^{-1}, and thus the correction factor $g = a/a_{Cox} = 0.86$. On average, from analysis of many fibers, $g = 0.84 \pm 0.17$.

The point of inflection between the initial shallower slope and the steeper final slope in Fig. 4 *b* corresponds to the time when bead retraction stopped. This suggested that bulk movement of fluid due to bead retraction (and the retraction

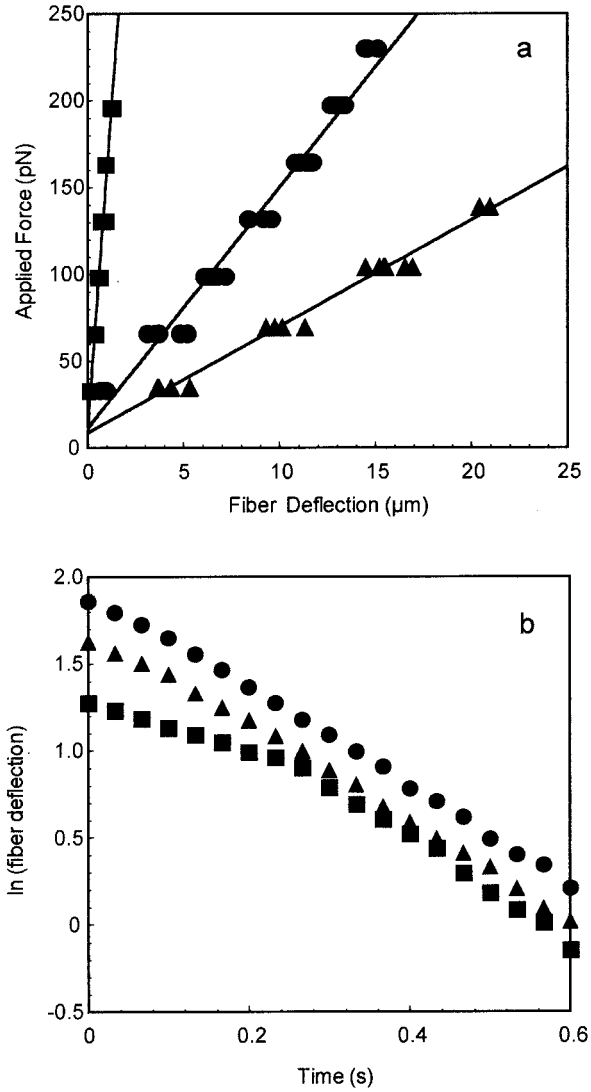

FIGURE 4 (*a*) Sample graphs of applied suction force on fibers versus equilibrium fiber deflection for three red blood cell piston calibration experiments. The slope of these curves gives the fiber spring constants: 147 pN · nm^{-1} (*squares*), 13.9 pN · nm^{-1} (*circles*), and 6.13 pN · nm^{-1} (*triangles*). The small non-zero force axis intercept is due to small pressure changes between the start and end of a 20-min run due to evaporation from the entry ports of the viewing chamber. (*b*) Natural logarithm of the fiber deflection after bond dissociation as a function of time for a set of adhesive events as the fiber returns to its rest position. The slope of the decay curves after 0.2 s are parallel with slope 3.00 ± 0.11 s^{-1}. This value can be used to compute k_{fiber}/a as described in the text. Before 0.2 s, the curve with the smallest initial deflection (*filled squares*) has a smaller initial slope due to hydrodynamic forces resulting from retraction of the bead.

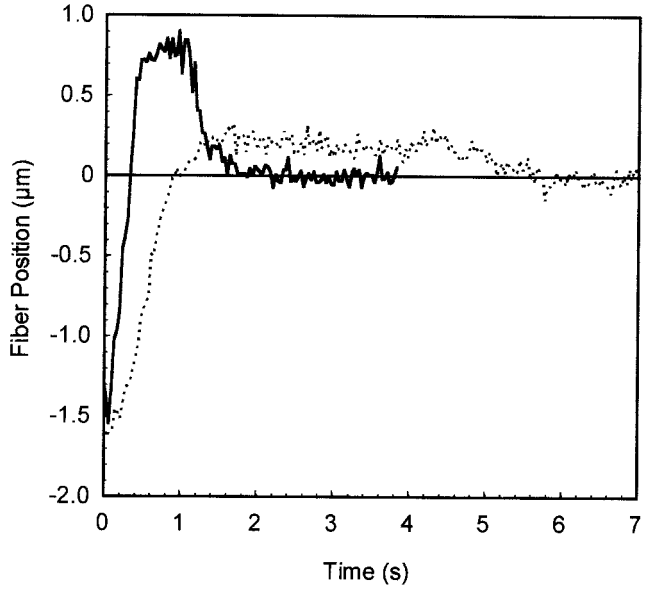

FIGURE 5 Sample fiber displacements versus time for apposition tests that did not result in bond formation. The curves represent bead retractions of 20 μm in 1.0 s (*solid line*; $V_{retract}$ = 20 μm s^{-1}) and 5.0 s (*dotted line*; $V_{retract}$ = 4 μm s^{-1}). The curves show maximum hydrodynamic deflections of 0.79 and 0.19 μm, respectively. After the bead retraction stops (at $t_{retract}$ = 1.0 or 5.0 s), the fibers relax back to their undeflected positions. Curves such as these can be used to obtain bead-retraction-induced force versus bead retraction velocity curves.

of the pipette that was used to hold it) applied an additional hydrodynamic drag on the fiber. This bead-retraction-induced hydrodynamic drag can also be quantified. Apposition tests that did not result in adhesive events were used to quantify the deflection induced by bead retraction. Fig. 5 shows sample fiber deflections for two different bead retraction velocities (20 and 4 μm s^{-1}). From their initial negative deflection (relative to the average fiber position after the bead had come to rest), fibers were deflected above the rest position by bead retraction. Note that once they were past the rest position, the bead and fiber were not in contact. For retraction velocities, $V_{retract}$ = 20 and 4 μm s^{-1}, the fibers came to rest at an equilibrium position corresponding to deflections from rest of 0.79 and 0.19 μm, respectively. This equilibrium position did not change during the period when the bead was retracting, $t_{retract}$. The lack of decrease in deflection confirmed that the retraction-induced deflection did not depend on proximity of the bead to the fiber. This implies that it is generalized fluid motion induced by movement of the multi-millimeter length of pipette stem inside the viewing chamber that causes the deflection. In all cases, immediately after the bead retractions stopped (at 1.0 s and 5.0 s for the two different cases), the fibers relaxed back to their rest positions. The equilibrium deflection during bead retraction can be used to determine the magnitude of the hydrodynamic effect. The final deflected positions can be multiplied by the fiber spring constant to give the hydrodynamic forces due to bead-retraction-induced flow. In Fig. 6, this force is plotted against retraction velocity. The curve is a straight line with slope 0.6 pN s μm^{-1}. It should be noted that this deflection is not a lubrication effect. By the time the constant fiber deflection appears, the bead and fiber are already many micrometers apart. The small bead-retraction-induced hy-

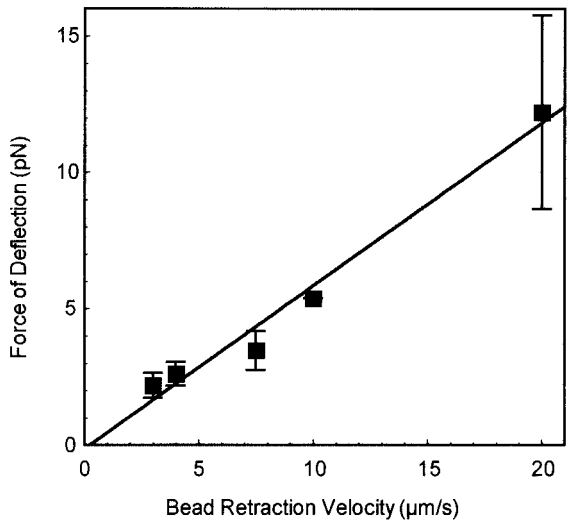

FIGURE 6 Bead-retraction-induced hydrodynamic force on fibers versus bead retraction velocity.

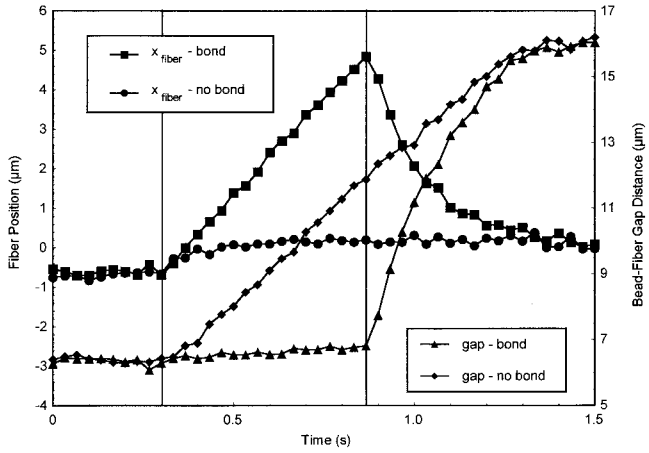

FIGURE 7 Graphs of fiber position and bead-fiber center-center gap distance for an adhesive event and a non-event. The fiber position for the bonded and nonbonded examples is shown on the left-hand axis, and gap distance is shown on the right-hand axis. The vertical lines show the start of bead retraction and the moment of bond dissociation. For the bonded example, the fiber position rises to a peak before dissociation, whereas the gap distance is constant (region between the vertical lines). In the nonbonded example, the gap distance increases smoothly and the fiber position remains essentially constant, rising slightly due to hydrodynamic forces generated by withdrawing the bead.

drodynamic force can be considered constant and added into f_o in Eq. 9 to include this effect in the force balance, although, since this extra force is velocity-dependent, it may also be added as a correction to the hydrodynamic coefficient, a.

Time distribution of dissociation

Frame by frame analysis of the fiber position as a function of time (at 30 frame s^{-1}) allows the time elapsed between the initiation of force ramp and the moment of break-up to be determined. Samples of fiber position and bead-fiber center-center gap distance for an adhesive event and a non-event are shown in Fig. 7. The 0.5- to 1.0-μm initial negative deflection of the fiber meant that the initial force on the bonds was negative—the surfaces were being pushed together by forces of 10 to 80 pN (depending on the fiber spring constant). For breakup to be observed, the bead-fiber gap distance had to grow to a value significantly larger than when the two were apposed. In tests that did not result in adhesive events, the bead and fiber separated gradually. Adhesive events, on the other hand, showed very little change in gap distance (area between vertical lines in Fig. 7), followed by a rapid increase to large separation after the moment of bond dissociation. The time of breakup, t_{break}, could be determined within an error of one video frame (± 0.033 s). The force acting at breakup was determined from $r_f t_{break}$. Fig. 8 shows a sample of the distributions of breakup as a function of applied force at breakup, obtained at a variety of loading rates. The number of events included in each of the 10 data sets varied from 8 to 66 (only five of these data sets are shown in Fig. 8). The $\langle t_{break} \rangle$ values were computed and converted into average forces at breakup using $r_f \langle t_{break} \rangle$. The distributions are tightly bunched at low force for slow loading rates, but are much broader, and have greater $\langle F_{break} \rangle$, at fast loading rates. Note that this broadening of the distribution does not reflect experimental error. It is a manifestation of the underlying stochastic distribution of breakup times that would be expected even under a constant force.

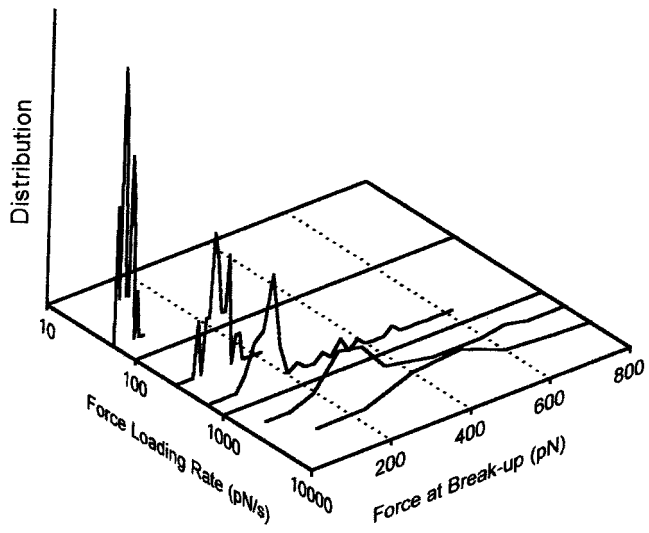

FIGURE 8 Curves showing the distribution of force at breakup for five different loading rates. The number of trials included at each different rate were: 25 at both 57 pN s^{-1} and 285 pN s^{-1}, 40 at 650 pN s^{-1}, 23 at 1800 pN s^{-1}, and 66 at 3600 pN s^{-1}. Note that the distributions broaden with increasing loading rate.

The average force at breakup, $\langle F_{break} \rangle$, is plotted versus ln r_f in Fig. 9. This curve appears to have as many as three different linear regions with different slopes. For the purposes of calculating the Bell model parameters, $\langle F_{break} \rangle$ provides a good estimator of f_{crit} for high loading rates, but not for the lowest loading rates (see Discussion). Thus the Bell parameters can be estimated from the slope and intercept of the $\langle F_{break} \rangle$ versus ln r_f best fit lines for the two faster loading rate regions shown in Fig. 9. These values are given in Table 1. The two branches have slopes of 85.2 and 256 pN for the loading rate ranges 200–1000 and 1000–5000 pN s^{-1}, respectively. As discussed in the Introduction, the slope of each branch is k_BT/r_o. Given that $k_BT = 4.1$ pN nm at room temperature, the r_o values are 0.048 and 0.016 nm for the loading rate ranges 200–1000 and 1000–5000 pN s^{-1}, respectively. The k_r^o value can be calculated from the slope and intercept, as shown in Eq. 5. The values are 0.72 and 2.2 s^{-1} for the loading rate ranges 200–1000 and 1000–5000 pN s^{-1}, respectively.

The primary source of error in this analysis comes from uncertainty in k_{fiber}. This value is computed using Eq. 6, which involves the third and fourth powers of L and D, respectively. Consequently, the propagated error can be quite significant. For example, an error of 3% (a typical measurement precision) leads to a propagated error of ~21% in k_{fiber}. Because the data from each loading rate were obtained with a different fiber, some variation in $\langle F_{break} \rangle$ is to be expected.

DISCUSSION

The experiments presented here demonstrate the usefulness of the fiber cantilever method for applying controlled, picoNewton-scale forces to receptor-ligand bonds. The method is simple to implement, easily tunable, and relatively inexpensive to construct. The advantage compared to AFM is that, like the biomembrane force probe, the device is optimized to apply small, physiologically relevant forces to adhesion molecules in a controlled manner. The trade-off is that the method lacks the nanoscale imaging capabilities of AFM. For the cantilever method to be properly implemented, however, the hydrodynamic forces acting on the fiber must be well understood. The results depicted in Figs. 4, 5, and 6 show that these forces can be understood and taken into account in the force balance on the fibers so that a true constant loading rate can be applied to receptor-ligand bonds.

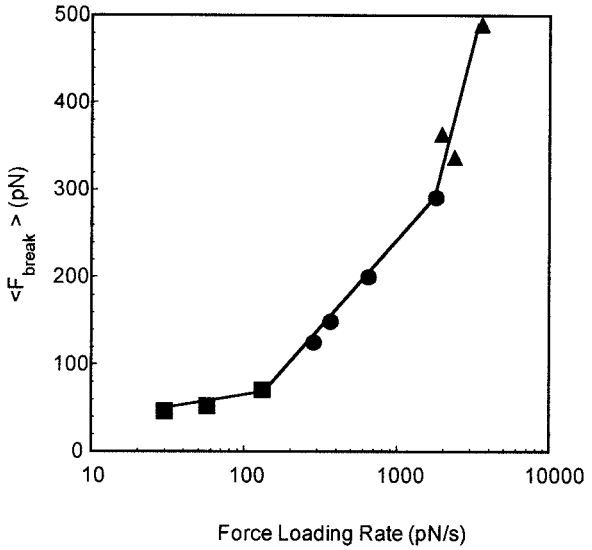

FIGURE 9 Average force at breakup versus logarithm of force loading rate (pN s^{-1}) for E-selectin-sLe^x bonding. The lines indicate separate straight segments that fit ranges of loading rate. The slopes and intercepts of these lines give the Bell model parameters shown in Table 1.

TABLE 1 Bell model parameters from $\langle F_{break} \rangle$ versus ln r_f

r_f range (pN s^{-1})	slope (pN)	r_o (nm)	intercept (pN)	k_r^o (s^{-1})
200–1000	85.2	0.048	−351	0.72
1000–5000	256	0.016	−1620	2.2

Monte Carlo analysis of parameter estimation

A number of questions arise out of the analysis of the dependence of $\langle F_{break} \rangle$ on ln r_f. First, given that in adhesion tests the desired adhesive event frequency was as high as 30%, what is the effect of the small number of multiple bonds that must have been present in some of the trials on the estimates of the $\langle F_{break} \rangle$? Multiple bonds increase the survival time of adhesive contacts, and thus the $\langle F_{break} \rangle$ will be an overestimate of the true average force for a single bond. Furthermore, what is the meaning of the multiple straight line branches in the $\langle F_{break} \rangle$ versus ln r_f curve? Lastly, the theory given in the Introduction applied to f_{crit}, the peak force, or mode, of the time distribution. We have instead used the mean force, $\langle F_{break} \rangle$, since it is a more robust estimator of central tendency of the distribution than the mode when the number of points in the distribution is not large. The validity of this substitution must be checked.

To analyze the time distributions in terms of the Bell model for the force dependence of reverse reaction rate, a simple Monte Carlo simulation of multiple bond dissociation (Tees et al., 1993) was adapted to the force loading regime used in the experiments (in this case, a linear ramp). In the simulation, the parameters are those for the Bell model: k_r^o, r_o, and the number of bonds, N_b, participating in the event. The initial N_b value is either set at a fixed value or chosen from a Poisson distribution. For each simulation time step, Δt, the instantaneous breakup probability, P_b, is computed from $P_b = 1 - \exp(-k_r(f)\Delta t)$, where f is the instantaneous applied force divided by the current number of bonds, which are assumed to support the force equally (Hammer and Apte, 1992). A random number between 0

and 1 is chosen for each bond remaining. If the number drawn is less than P_b, then N_b is reduced by 1 and the force per bond acting on the remaining bonds is recalculated. The cycle of force computation, probability calculation, and breakup testing is repeated until N_b goes to zero, or until a final cutoff time, corresponding to the end of the loading phase of the loading cycle, is reached. Statistics for average breakup time, $\langle t_{break}\rangle$, or $\langle F_{break}\rangle$ can then be computed using different parameter sets.

The results of $\langle F_{break}\rangle$ versus ln r_f from a Monte Carlo simulation with underlying Bell model parameters $r_o = 0.03$ nm and $k_r^o = 1.0\ s^{-1}$ are shown in Fig. 10. The $\langle t_{break}\rangle$ for 10,000 simulated bead-fiber apposition tests was computed for a range of loading rates from 1 to 10,000 pN s^{-1}. Simulations at all loading rates were performed with the Bell model parameters $r_o = 0.03$ nm and $k_r^o = 1.0\ s^{-1}$, and thus the estimates of these parameters produced by the slope and intercept of $\langle F_{break}\rangle$ versus ln r_f can be compared with the true values. In the different simulations, the number of bonds was varied. The number of bonds was either fixed at $N_b = 1$ or chosen from a Poisson distribution with $\langle N_b\rangle$ (including $N_b = 0$) = 0.1, 0.2, 0.4, and 0.8. These average bond numbers represent small but increasing numbers of multiple bonds. For $\langle N_b\rangle = 0.1$, there is 10% adhesion, and only 5% of positive tests involve multiple bonds ($N_b > 1$). For $\langle N_b\rangle = 0.8$, on the other hand, there is 55% adhesion, and 35% of positive tests involve multiple bonds (see Appendix A). The results indicate that for $r_f > 200$ pN s^{-1}, the curves are relatively straight. For $r_f < 200^{pNs^{-1}}$, however, the curves for single or multiple bonds all decrease in slope as r_f decreases and $\langle F_{break}\rangle$ goes to zero at very low loading rates. This result is expected (Evans and Ritchie, 1997) and can be demonstrated using the probability distribution as a function of time from reliability theory:

$$p_r(t, f) = k_r^o \exp\left[\frac{r_o r_f t}{kT}\right]\exp\left[-\frac{k_r^o kT}{r_f}\left\{\exp\left(\frac{r_o r_f t}{kT}\right) - 1\right\}\right], \tag{11}$$

The mean of this distribution is given by

$$\langle f_{break}\rangle = r_f\langle t_b\rangle = r_f\int tp(t, f)dt = \frac{kT}{r_o}\exp\left[\frac{k_r^o kT}{r_f r_o}\right]E_1\left(\frac{k_r^o kT}{r_f r_o}\right), \tag{12}$$

where $E_1(x)$ is the exponential integral, $E_1(x) = \int_1^\infty \exp(xt)/t\,dt$ (Abramowitz and Stegun, 1965). The dependence of $\langle F_{break}\rangle$ on ln r_f, given by Eq. 12, is plotted in Fig. 10 (the curve labeled $N_b = 1$ theory) and it matches the Monte Carlo results extremely well.

Table 2 shows the effect of bond number on parameter estimation for values of $r_f > 200$ pN s^{-1} in Fig. 10. The slopes and intercepts lead to Bell model parameters that all agree well with the values $r_o = 0.03$ nm and $k_r^o = 1.0\ s^{-1}$ used to produce the curves. Even in the case where $\langle N_b\rangle = 0.8$, in which we expect 35% multiple bonds, the estimated r_o is only 0.027 (a 10% reduction from the correct value). The k_r^o value is also weakly affected (12% reduction from theoretical value for a single bond).

Fig. 10 further indicates that the use of mean force (or peak observed force) for low loading rates (<200 pN s^{-1}) will lead to poor estimation of the Bell model parameters, since the slope of the curves decreases to zero below this value. Both theory and simulation show that for this range of loading rates, $\langle F_{break}\rangle$ goes to zero, as does the mode of the force distribution. To investigate this further, one can fit the theoretical equation given in Eq. 12 for $\langle F_{break}\rangle$ for single bond dissociation in the presence of a linear ramp of force to the data in Fig. 9. Using a Levenberg-Marquardt non-linear least squares fitting program (Press et al., 1986), the Bell model parameters that best fit all the data for $\langle F_{break}\rangle$ versus r_f were found to be $k_r^o = 0.82\ s^{-1}$ and $r_o = 0.034$ nm. The $\langle F_{break}\rangle$ versus r_f curve computed from these parameters is shown in Fig. 11 superimposed on the data from Fig. 9. The fit is very good over much of the loading rate range for which data are available. The only divergence

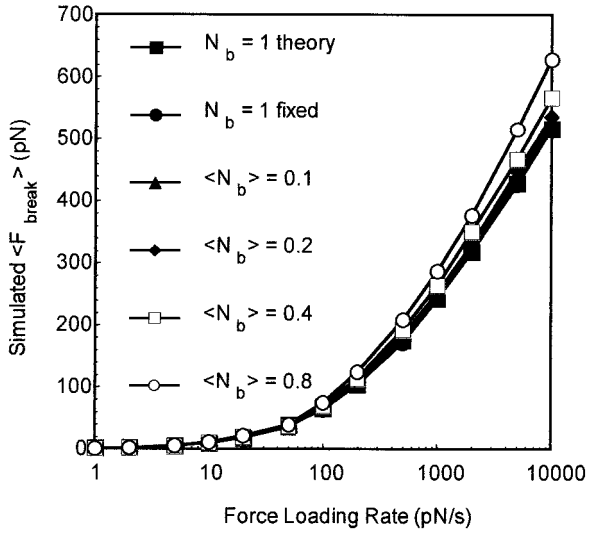

FIGURE 10 Graph of simulated average force at breakup versus logarithm of simulated loading rate for different numbers of multiple bonds. Simulation results agree well with theoretical predictions (Eq. 12), except at the highest bonding probabilities ($\langle N_b\rangle > 0.4$) and are consistent with experimental results.

TABLE 2 Effect of multiple bonds on Bell model parameter estimates. Actual parameters: $r_o = 0.03$ nm and $k_r^o = 1.0\ s^{-1}$

$\langle N_b\rangle$	slope (pN)	r_o (nm)	intercept (pN)	k_r^o (s^{-1})
1 (Theory)	119	0.034	−586	1.16
1 (fixed)	119	0.034	−583	1.13
0.1	122	0.33	−604	1.16
0.2	124	0.033	−611	1.11
0.4	131	0.031	−645	1.05
0.8	149	0.027	−748	1.02

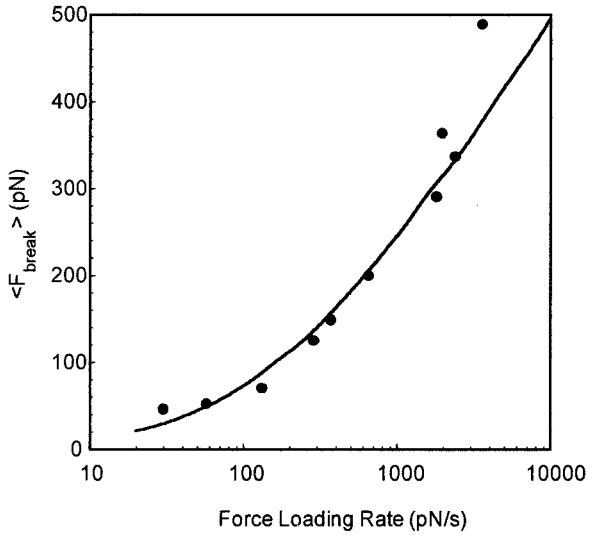

FIGURE 11 Data from Fig. 9 with the superimposed *solid line* indicating $\langle F_{break}\rangle$ versus ln r_f computed from Eq. 12 using the best fit Bell model parameters $k_r^o = 0.82\ s^{-1}$ and $r_o = 0.034$ nm.

is at very high loading rate, where there is the suggestion that a different, steeper slope, indicative of another set of Bell model parameters, may exist. A fit to the same data, but ignoring the final, most divergent point, leads to $r_o = 0.039$ nm and $k_r^o = 0.73\ s^{-1}$ (fit not shown). These values are midway between the parameters derived from the two faster loading rate segments of $\langle F_{break}\rangle$ versus r_f given in Table 1. The goodness of the fit to a single set of Bell model parameters suggests that there are several possible valid methods for fitting parameters to the data.

In light of the preceding discussion, it appears unlikely that the lower slope of the $\langle F_{break}\rangle$ versus ln r_f curve in the slow loading rate regime ($50 < r_f < 200$ pN s^{-1}; Fig. 9) represents a separate set of model parameters. Rather, the reduced slope is consistent with a single parameter set spanning the slow to intermediate loading regimes. Thus, the E-selectin-sLe^x data in the 50–200 pN s^{-1} loading rate range appear to be consistent with the same Bell model parameters as the 200–1000 pN s^{-1} range. The two faster loading rate ranges, which give $r_o = 0.016$ and 0.048 nm, are in the robust estimation range, and one expects these values to be consistent with two distinct parameter sets that apply to the different loading rate ranges.

A final conclusion for the Monte Carlo analysis is that for the larger loading rates (>200 pN s^{-1}), the mean and mode of the time distributions approach one another, and the mean can serve as an accurate indicator of the mode, thus validating the use of $\langle F_{break}\rangle$ in the analysis of the data. This is evident from the results shown in Table 2. The value of k_r^o was set to 1.0 s^{-1}, and distributions of force at breakup were calculated at different loading rates. When the average values of the calculated distributions were used to recalculate the Bell parameters via Eq. 5 (with $\langle F_{break}\rangle$ substituted for f_{crit}), the calculated value agreed with the original k_r^o used to generate the distributions within 16%. The ability to use the average value of the force at breakup, rather than the mode of the distribution, to calculate the Bell parameters greatly facilitates data acquisition and analysis, particularly because a much larger number of measurements is needed to accurately determine the mode (as opposed to the mean) of the distribution at each loading rate.

Nonspecific adhesion

As shown in Fig. 3, it proved impossible to reduce nonspecific adhesion to negligible levels in these experiments. To address the uncertainty that nonspecific adhesion caused in parameter estimation, the slope of $\langle F_{break}\rangle$ versus ln r_f curves for the nonspecific tests was measured and an "effective r_o" was calculated for nonspecific adhesion. For $50 < r_f < 1100$ pN s^{-1}, the curve was linear with $\langle F_{break}\rangle = 38 \ln r_f - 105$ (data not shown). This implies that $r_o = 0.11$ nm and $k_r^o = 0.39\ s^{-1}$ for nonspecific adhesion events. A simulation was developed that allowed a combination of the Bell model parameters for nonspecific and specific adhesion to be simulated (parameters for the latter were taken from the experimental $200 < r_f < 1000$ pN s^{-1} loading rate range). Analysis of simulated curves of $\langle F_{break}\rangle$ versus ln r_f led to 7% higher r_o values when 10% of events were nonspecific, and 18% higher r_o values if 30% of events were nonspecific. This analysis serves as an example of how parameters for specific adhesion may be recovered accurately even in the presence of a significant nonspecific background.

Implications for E-selectin-sLe^x adhesive phenotype

The Monte Carlo analysis indicates that for high and intermediate loading rates the Bell model parameter estimates derived from the slopes of individual straight segments of $\langle F_{break}\rangle$ versus r_f curves are robust and accurate to within ~10% of the correct value for that segment. At the lowest loading rates, estimates of the parameters are inaccurate, and results for loading rates of 50 to 200 pN s^{-1} are an extension of the middle range of loading rate. The k_r^o values obtained at intermediate and high loading rates (0.72 and 2.2 s^{-1}) are both consistent with measurements of selectin reverse reaction rates reported in the literature. Reverse reaction rates under zero force have been determined for P-selectin-PSGL-1 to be $1.4 \pm 0.1\ s^{-1}$ using surface plasmon resonance (Mehta et al., 1998). Neutrophil tethering duration studies yield values of 0.95 s^{-1} for P-selectin-PSGL-1 and 0.70 s^{-1} (Alon et al., 1997), 0.5 s^{-1} (Kaplanski et al., 1993), or $2.6 \pm 0.45\ s^{-1}$ (Smith et al., 1999) for E-selectin and its glycoprotein ligand. These latter values

agree well with the value we obtain for sLe^x/E-selectin substrates and loading rates <1000 pN s^{-1}.

Values for the Bell model parameter, r_o, obtained in the present study are also consistent with those found using other methods. For comparison, Alon et al. (1997) used an adhesive tether duration assay in a parallel plate flow chamber and found that $r_o = 0.03$ nm for E-selectin and 0.049 nm for P-selectin adhering to their natural ligands on neutrophils. Smith et al. (1999) found values of 0.039 nm and 0.018 nm for P- and E-selectin, respectively, using the same type of assay but with arrest duration determined using a high-speed camera to allow very short-lived events to be captured. These values for E-selectin fall between the values we obtain at high and intermediate loading rates (0.048 and 0.016 nm) and agree very closely with the value obtained by fitting the exact function for the mean force versus ln r_f (Fig. 11): $r_o = 0.034$ nm. The present results are also consistent with molecular constants obtained in cell-free rolling experiments (Brunk and Hammer, 1997). An order of magnitude estimate for the r_f in leukocyte rolling experiments is ~100 pN applied within times that can vary from as little as 10 ms to as much as 100 ms = 10^3 to 10^4 pN s^{-1}. In view of this fact, it is interesting that the $r_o = 0.016$ nm value found for this loading rate range agrees with best fits to cell-free rolling experiments from adhesive dynamics simulations of leukocyte rolling (Chang et al., 2000b).

Different ranges of force and different Bell parameters have been found for other molecular pairs or for selectins measured by another method. Fritz et al. (1998) found a value of $r_o = 0.25$ nm for P-selectin using AFM, and measured corresponding forces for bond breakage that were significantly smaller than the ones we report here (Fritz et al., 1998). The reasons for the discrepancy between our results and theirs (and between their results and Bell parameters estimated from cell rolling experiments) are not clear, but may relate to differences in the state of the molecules or the valency of bonding in the different systems. (See below for a discussion of multivalent bonding.) Streptavidin/biotin bonds (Merkel et al., 1999) and antigen/antibody binding (Hinterdorfer et al., 1996) also display smaller values for the forces at breakage at similar loading rates. These may be attributed to differences in the chemical nature of the molecules involved, the binding of which may have markedly different dependence on force. The Monte Carlo simulation data shown in Fig. 10 demonstrate that the forces observed in the present study are to be expected, given the Bell model parameters estimated from cell rolling experiments and the loading rates that were applied.

The agreement between parameter estimates using this technique and cell arrest duration assays indicate that sLe^x alone could account completely for the behavior of E-selectin-mediated bonding during cell rolling. This could explain why it has been so difficult to identify a unique glycoprotein ligand for E-selectin; it is possible that sialyl $Lewis^x$ (which is expressed on many cell surface glycoproteins) is, indeed, the physiological ligand for E-selectin.

Merkel et al. (1999) applied a force spectroscopic analysis similar to that performed here to avidin-biotin bonds. They also obtained a series of linear regimes leading to a series of values for the Bell model parameter r_o. This was interpreted as the radial position of transition states in the one-dimensional bonding potential that prevents the molecules from diffusing apart. The transition state positions of 0.12, 0.4, and 3.0 nm that they obtained for avidin-biotin corresponded with features in the known three-dimensional structure of the binding pocket and agreed with transition states found using molecular dynamics simulations of dissociation. This correspondence lends credence to the notion that the Bell model parameter truly represents a transition state position. This identification is harder to reconcile with the Bell model parameters that are typically obtained for the selectins. Here, r_o values have been consistently found to be small fractions of an Angstrom. It strains credulity to imagine that a true physical transition state could occur at a distance that is a small fraction of the radius of a hydrogen atom. It is perhaps instructive to recall that the magnitude of r_o describes how strongly the reverse reaction rate varies with force. A small value indicates that for a large range of loading rates, the reverse reaction rate depends relatively weakly on force. In this way, perhaps due to conformational changes in the selectins as the molecules are stressed, the interaction potential could appear to change very little with applied force. It is possible to reconcile this notion with more plausible values for transition state positions using a vector orientation of the transition state range. If the direction of force application, $\mathbf{f}$, and the vector transition state range, $\mathbf{r}$, are at some angle, θ, to one another, then the apparent $r_o = \|\mathbf{r}\| \cos\theta$. The Bell model parameters obtained for the selectins would, thus, be proportional to the positions of transition states, but may or may not represent the actual transition state distances depending on the parameter, θ.

Multivalent binding

Another possible explanation for the small value of r_o is that the unitary events observed in the present study may each involve the formation of two or more bonds between each receptor and ligand. In Monte Carlo simulations, unbinding of multiple bonds also leads to straight lines on $\langle F_{break} \rangle$ versus ln r_f diagrams, but the curves are steeper and left-shifted compared to singly bonded systems. For example, if the underlying r_o value for single bond breakup is 0.1 nm, simulations show that the r_o value measured from $\langle F_{break} \rangle$ versus ln r_f analysis will be $r_o = 0.11$ nm if all $N_b = 1$, $r_o = 0.07$ nm if $N_b = 2$, and $r_o = 0.05$ nm if $N_b = 3$. Therefore, the apparent r_o in such a multiply bonded system could be significantly less than the physical value of r_o for the underlying individual bonds. Such multiple bonding events may be plausible in the present system, because both the

E-selectin chimera and the sLe^x-PAA-biotin polymer are multivalent. Considering the possibility that one E-selectin molecule might bind multiple copies of sLe^x, we note that the distance between neighboring tetrasaccharides in the sLe^x-PAA-biotin polymer is very small. There are ~20 along the length of a 30-kd polymer—perhaps 20 nm long—implying a spacing of ~1 nm. Given this scale, a single E-selectin molecule in close proximity to an sLe^x-PAA-biotin polymer clearly sees a forest of sLe^x. Cantilever measurements do not enable us to determine whether a single E-selectin molecule can bind to multiple copies of sLe^x, but the low frequency with which binding events occur indicates that if such multiple binding did occur, it would have to behave as a single binding event, indistinguishable from binding to a single sLe^x moiety. Ultrastructural data should eventually provide an answer to this question, but the structure of E-selectin bound to sLe^x is not known at this time. The structure of mannose binding protein mutated to resemble the E-selectin binding pocket has been solved in conjugation with ligand, and in this case only one bound sLe^x was found (Ng and Weis, 1997). Nevertheless, until more definitive ultrastructural data are obtained, the possibility that the E-selectin interacts with multiple copies of sLe^x cannot be discounted.

The possibility that the two arms of the E-selectin chimera bind simultaneously to multiple ligands seems less plausible. The larger separation distance between the "arms" of the chimera (10–20 nm) is comparable to the interchimera separation distance. In addition, the random orientation of the chimera might prevent one of the two arms from interacting with ligand, and in the case that both arms can interact, the flexibility of the Fab arms should allow each arm to behave independently, equivalent to separate adhesive molecules during adhesive bond formation.

The agreement between the values obtained in the present study and values for r_o estimated from cell rolling experiments (Smith et al., 1999) indicates that the bonding mechanism at work in these cantilever studies is relevant to molecular events during cell rolling. In particular, if multiple bond formation does account for the small value of r_o observed for E-selectin-sLe^x interactions, then it would appear likely that E-selectin binding in vivo must also involve multiple copies of sLe^x. We have recently used the adhesive dynamics simulation technique to show that only certain combinations of Bell model parameters lead to adhesive behaviors such as rolling (Chang et al., 2000). A single sLe^x-E-selectin bond has a flat binding face consisting of a number of hydrogen bonds that should lead to an r_o value of ~1 Å. The formation of unitary multiple bonds could, thus, be a way of changing the effective Bell model parameters in such a way that rolling is made possible. Whether this possibility will be supported by direct ultrastructural studies remains to be seen.

CONCLUSION

The results shown here demonstrate the usefulness of microcantilevers for studying physiologically relevant bond kinetics. When the hydrodynamic forces acting on fiber cantilevers are taken into account, a constant loading rate can be applied to receptor-ligand bonds. The average force at the moment of bond dissociation can be measured as a function of loading rate, and the resulting analysis yields the parameters in the Bell model for the force dependence of the reverse reaction rate. The Bell model parameters obtained for E-selectin and its carbohydrate ligand sLe^x are consistent with those found using independent methods, and match the values needed to facilitate rolling adhesion of receptor-coated cells to ligand-covered surfaces predicted from adhesive dynamics simulations of cell adhesion to surfaces. The agreement between experiment and simulation suggests that the microcantilever device provides a useful method for measuring the force dependence of reverse reaction rates and hence for predicting adhesive phenotype. Finally, the parameter estimates from these experiments using E-selectin and sLe^x agree well with those from assays that use E-selectin binding to its putative glycoprotein ligand. This suggests that sialyl $Lewis^x$ could, indeed, be the physiological ligand for E-selectin.

APPENDIX A

Poisson Distribution

It has become standard practice to use the frequency of bonding events as an assessment of the number of bonds present during adhesive events. The number of bonds, N_b, formed during cell adhesive contacts has long been thought to follow a Poisson distribution (Capo et al., 1982). The argument has since been extended to quantitative bond number assessment in a number of papers (Chesla et al., 1998; Merkel et al., 1999). Assume that bonds follow the Poisson distribution:

$$P(N_b) = \frac{\lambda^{N_b} \exp[-\lambda]}{N_b!} \tag{A1}$$

where λ is a parameter that turns out to be the mean bond number, $\langle N_b \rangle$ (standard deviation is $N_b^{1/2}$). Assume further that any adhesive test that does not lead to bond formation (as assessed by the adhesion assay) is a manifestation of $N_b = 0$. It then follows that since $P(N_b = 0) = \langle N_b \rangle^o e^{-\langle Nb \rangle}/0! = e^{-\langle Nb \rangle}$, $\langle N_b \rangle = -\ln P(N_b = 0)$. In this way, the parameter in the Poisson distribution, $\langle N_b \rangle$, can be computed from the fraction of tests that led to no adhesive event $P(N_b = 0)$, or equivalently, from $(1 - P_a)$ where P_a is the fraction of tests that did result in adhesive events.

Once $\langle N_b \rangle$ is known, the fraction of tests that have a given number of bonds can be computed using Eq. A1. The fraction of events that have a given number of bonds $= P(N_b | N_b > 0)$ is given by:

$$\begin{aligned} P(N_b | N_b > 0) &= \frac{P(N_b)}{(1 - P(0))} = \frac{\langle N_b \rangle^{N_b}}{((\exp\langle N_b \rangle - 1) N_b!)} \\ &= \frac{(1 - P_a)(-\ln(1 - P_a))^{N_b}}{P_a N_b!}. \end{aligned} \tag{A2}$$

In this paper the $\langle N_b \rangle$ is computed using all values of N_b, including the $N_b = 0$ values. If desired, however, the average number of bonds excluding $N_b = 0$ bonds, $\langle N_b | N_b > 0 \rangle$, can also be computed:

$$\langle N_b | N_b > 0 \rangle = \frac{\langle N_b \rangle}{(1 - \exp - \langle N_b \rangle)}. \quad \text{(A3)}$$

We thank Mr. Richard Bauserman for expert technical advice and Dr. Robert Hochmuth for valuable suggestions. The authors particularly wish to acknowledge Dr. Evan Evans for developing the method of analysis and suggesting the explanation for the extremely small transition state ranges given in the Discussion.

This work was supported by grant HL 18208 from the National Institutes of Health. Additional support for D. F. J. T. was provided by the Fonds pour la Formation de Chercheurs et l'Aide à la Recherche of the government of Québec.

REFERENCES

Abramowitz, M., and I. A. Stegun. 1965. Handbook of Mathematical Functions. Dover Publication, Inc., New York.

Alon, R., S. Chen, K. D. Puri, E. B. Finger, and T. A. Springer. 1997. The kinetics of L-selectin tethers and the mechanics of selectin-mediated rolling. *J. Cell Biol.* 138:1169–1180.

Alon, R., D. A. Hammer, and T. A. Springer. 1995. Lifetime of the P-selectin-carbohydrate bond and its response to tensile force in hydrodynamic flow. *Nature (London).* 374:539–542.

Batchelor, G. K. 1970. Slender-body theory for particles of arbitrary cross-section in Stokes flow. *J. Fluid Mech.* 44:419–440.

Beckmann, P. 1967. Probability in Communication Engineering. Harcourt, Brace & World, Inc., New York.

Bell, G. I. 1978. Models for the specific adhesion of cells to cells. *Science.* 200:618–627.

Bischoff, J. 1997. Cell adhesion and angiogenesis. *J. Clin. Invest.* 99: 373–376.

Bruinsma, R. 1997. Les liaisons dangereuses: adhesion molecules do it statistically. *Proc. Natl. Acad. Sci. USA.* 94:375–376.

Brunk, D. K., D. J. Goetz, and D. A. Hammer. 1996. Sialyl lewis^x/E-selectin-mediated rolling in a cell-free system. *Biophys. J.* 71: 2902–2907.

Brunk, D. K., and D. A. Hammer. 1997. Quantifying rolling adhesion with a cell-free assay: E-selectin and its carbohydrate ligands. *Biophys. J.* 72:2820–2833.

Capo, C., F. Garrouste, A.-M. Benoliel, P. Bongrand, A. Ryter, and G. I. Bell. 1982. Concanavalin-A-mediated thymocyte agglutination: a model for a quantitative study of cell adhesion. *J. Cell Sci.* 56:21–48.

Chang, K.-C., D. F. J. Tees, and D. A. Hammer. 2000. The state diagram for cell adhesion under flow: leukocyte rolling and firm adhesion. *Proc. Natl. Acad. Sci. USA.* 97:11262–11267.

Chang, K.-C., and D. A. Hammer. 2000b. Adhesive dynamic simulations of Sialyl-Lewis*/E-selectin-mediated rolling in a cell-free system. *Biophys. J.* 79:1891–1902.

Chesla, S. E., P. Selvaraj, and C. Zhu. 1998. Measuring two-dimensional receptor-ligand binding kinetics by micropipette. *Biophys. J.* 75: 1553–1572.

Colman, R. W., J. Hirsch, V. J. Marder, and E. W. Salzman. 1994. Hemostasis and thrombosis: basic principles and clinical practice. J. B. Lippincott Co., Philadelphia.

Cox, R. G. 1970. The motion of long slender bodies in a viscous fluid. 1. General theory. *J. Fluid Mech.* 44:791–810.

Dembo, M., D. C. Torney, K. Saxman, and D. Hammer. 1988. The reaction limited kinetics of membrane-to-surface adhesion and detachment. *Proc. Royal Soc. Lond. B. Biol. Sci.* 234:55–83.

Evans, E., D. Berk, and A. Leung. 1991. Detachment of agglutinin-bonded red blood cells. I. Forces to rupture molecular-point attachments. *Biophys. J.* 59:838–848.

Evans, E., and K. Ritchie. 1997. Dynamic strength of molecular adhesion bonds. *Biophys. J.* 72:1541–1555.

Florin, E.-L., V. T. Moy, and H. E. Gaub. 1994. Adhesion forces between individual ligand-receptor pairs. *Science.* 264:415–417.

Fritz, J., A. G. Katopodis, F. Kolbinger, and D. Anselmetti. 1998. Force-mediated kinetics of single P-selectin/ligand complexes observed by atomic force microscopy. *Proc. Natl. Acad. Sci. USA.* 95:12783–12288.

García, A. J., F. Huber, and D. Boettiger. 1998. Force required to break $\alpha_5\beta_1$ integrin-fibronectin bonds in intact adherent cells is sensitive to integrin activation state. *J. Biol. Chem.* 273:10988–10993.

Gibson, R. F. 1994. Principles of composite material mechanics. McGraw Hill, New York.

Hammer, D. A., and S. M. Apte. 1992. Simulation of cell rolling and adhesion on surfaces in shear flow: general results and analysis of selectin-mediated neutrophil adhesion. *Biophys. J.* 63:35–57.

Hänggi, P., P. Talkner, and M. Borkevec. 1990. Reaction-rate theory: fifty years after Kramers. *Rev. Mod. Phys.* 62:251–341.

Hinterdorfer, P., W. Baumgartner, H. J. Gruber, K. Schilcher, and H. Schindler. 1996. Detection and localization of individual antibody-antigen recognition events by atomic force microscopy. *Proc. Natl. Acad. Sci. USA.* 93:3477–3481.

Hwang, W. C., and R. E. Waugh. 1997. Energy of dissociation of lipid bilayer from the membrane skeleton of red blood cells. *Biophys. J.* 72:2669–2678.

Hyer, M. W. 1998. Stress analysis of fiber-reinforced composite materials. WCB McGraw Hill, New York.

Jones, F. R. 1994. Handbook of Polymer-Fibre Composites. Longman Scientific & Technical, Harlow, UK.

Kansas, G. S. 1996. Selectins and their ligands: current concepts and controversies. *Blood.* 88:3259–3287.

Kaplanski, G., C. Farnarier, O. Tissot, A. Pierres, A.-M. Benoliel, M.-C. Alessi, S. Kaplanski, and P. Bongrand. 1993. Granulocyte-endothelium initial adhesion: analysis of transient binding events mediated by E-selectin in a laminar shear flow. *Biophys. J.* 64:1922–1933.

Kramers, H. A. 1940. Brownian motion in a field of force and the diffusion model of chemical reactions. *Physica.* 7:284–302.

Lafrenie, R. M., M. R. Buchanan, and F. W. Orr. 1993. Adhesion molecules and their role in cancer metastasis. *Cell Biophys.* 23:3–89.

Lawrence, M. B., and T. A. Springer. 1991. Leukocytes roll on a selectin at physiological flow rates: distinction from and prerequisite for adhesion through integrins. *Cell.* 65:859–874.

Mehta, P., R. D. Cummings, and R. P. McEver. 1998. Affinity and kinetic analysis of P-selectin binding to P-selectin glycoprotein ligand-1. *J. Biol. Chem.* 273:32506–32513.

Merkel, R., P. Nassoy, A. Leung, K. Ritchie, and E. Evans. 1999. Energy landscapes of receptor-ligand bonds explored with dynamic force spectroscopy. *Nature (London).* 397:50–53.

Moore, J. H., C. C. Davis, and M. A. Coplan. 1989. Building Scientific Apparatus: A Practical Guide to Design and Construction. Addison-Wesley Publishing Co., Reading, MA.

Ng, K. K.-S., and W. I. Weis. 1997. Structure of a selectin-like mutant of mannose-binding protein complexed with sialylated and sulfated lewisx oligosaccharides. *Biochemistry.* 36:979–988.

Pierres, A., A.-M. Benoliel, and P. Bongrand. 1995. Measuring the lifetime of bonds made between surface-linked molecules. *J. Biol. Chem.* 270: 26586–26592.

Press, W. H., B. P. Flannery, S. A. Teukolsky, and W. T. Vetterling. 1986. Numerical Recipes. Cambridge University Press, New York.

Radmacher, M., J. P. Cleveland, M. Fritz, H. G. Hansma, and P. K. Hansma. 1994. Mapping interaction forces with the atomic force microscope. *Biophys. J.* 66:2159–2165.

Shao, J.-Y., H. P. Ting-Beall, and R. M. Hochmuth. 1998. Static and dynamic lengths of neutrophil microvilli. *Proc. Natl. Acad. Sci. USA.* 95:6797–6802.

Smith, M. J., E. L. Berg, and M. B. Lawrence. 1999. A direct comparison of selectin-mediated transient, adhesive events using high temporal resolution. *Biophys. J.* 77:3371–3383.

Springer, T. A. 1994. Traffic signals for lymphocyte recirculation and leukocyte emigration: the multistep paradigm. *Cell.* 76:301–314.

Tees, D. F. J., O. Coenen, and H. L. Goldsmith. 1993. Interaction forces between red cells agglutinated by antibody IV. Time and force dependence of breakup. *Biophys. J.* 65:1318–1334.

Tha, S. P., J. Shuster, and H. L. Goldsmith. 1986. Interaction forces between red cells agglutinated by antibody II. Measurement of hydrodynamic force of breakup. *Biophys. J.* 50:1117–1126.

Varki, A. 1994. Selectin ligands. *Proc. Natl. Acad. Sci. USA.* 91: 7390–7397.

von Andrian, U. H., J. D. Chambers, L. M. McEvoy, R. F. Bargatze, K.-E. Arfors, and E. C. Butcher. 1991. Two-step model of leukocyte-endothelial cell interactions in inflammation: distinct roles for LECAM-1 and leukocyte $\beta 2$ integrins in vivo. *Proc. Natl. Acad. Sci. USA.* 88:7538–7542.